JATIS Journal of Astronomical Telescopes, Instruments, and Systems

RESEARCH PAPER

# High-angular resolution and high contrast observations from Y to L band at the Very Large Telescope Interferometer with the Asgard Instrumental suite

Marc-Antoine Martinod,[a,*] Denis Defrère,[a] Michael Ireland,[b] Stefan Kraus,[c] Frantz Martinache,[d] Peter Tuthill,[e] Azzurra Bigioli,[a] Emilie Bouzerand,[f] Julia Bryant,[e] Sorabh Chhabra,[c] Benjamin Courtney-Barrer,[b] Fred Crous,[e] Nick Cvetojevic,[d] Colin Dandumont,[g] Steve Ertel,[h,i] Tyler Gardner,[c] Germain Garreau,[a] Adrian M. Glauser,[f] Lucas Labadie,[j] Tiphaine Lagadec,[b] Romain Laugier,[a] Alexandra Mazzoli,[g] Daniel Mortimer,[c] Barnaby Norris,[e] Gert Raskin,[a] Gordon Robertson,[e] Ahmed Sanny,[j,k] and Adam Taras[e]

[a]KU Leuven, Institute of Astronomy, Leuven, Belgium
[b]The Australian National University, Canberra, Australia
[c]University of Exeter, School of Physics and Astronomy, Exeter, United Kingdom
[d]Observatoire de la Côte d'Azur, Nice, France
[e]University of Sydney, Sydney Institute for Astronomy, School of Physics, Camperdown, New South Wales, Australia
[f]ETH Zurich, Institute for Particle Physics and Astrophysics, Zurich, Switzerland
[g]University of Liège, Space Sciences, Technologies & Astrophysics Research (STAR) Institute, Liège, Belgium
[h]University of Arizona, Department of Astronomy and Steward Observatory, Tucson, Arizona, United States
[i]Large Binocular Telescope Observatory, Tucson, Arizona, United States
[j]Universität zu Köln, I. Physikalisches Institut, Cologne, Germany
[k]Macquarie University, School of Mathematical and Physical Sciences, MQ Photonics Research Centre, Macquarie Park, New South Wales, Australia

**ABSTRACT.** European Southern Observatory (ESO)'s Very Large Telescope Interferometer (VLTI), Paranal, Chile, is one of the most proficient observatories in the world for high angular resolution astronomy. It has hosted several interferometric instruments operating in various bandwidths in the infrared. As a result, the VLTI has yielded countless discoveries and technological breakthroughs. We propose to ESO a new concept for a visitor instrument for the VLTI: Asgard. It is an instrumental suite comprised of four natively collaborating instruments: High-Efficiency Multiaxial Do-it ALL Recombiner (HEIMDALLR), an all-in-one instrument performing both fringe tracking and stellar interferometry with the same optics; Baldr, a Strehl optimizer; Beam-combination Instrument for studying the Formation and fundamental paRameters of Stars and planeTary systems (BIFROST), a combiner whose main science case is studying the formation processes and properties of stellar and planetary systems; and Nulling Observations of dusT and planeTs (NOTT), a nulling interferometer dedicated to imaging young nearby planetary systems in the L band. The overlap between the science cases across different spectral bands yields the idea of making the instruments complementary to deliver sensitivity and accuracy from the J to L bands. Asgard is to be set on the former AMBER optical table. Its control architecture is a hybrid between custom and ESO-compliant developments to benefit from the flexibility offered to a visitor instrument and foresee a deeper long-term integration into VLTI for an opening to the community.

 [DOI: 10.1117/1.JATIS.9.2.025007]

*Address all correspondence to Marc-Antoine Martinod, marc-antoine.martinod@kuleuven.be

**Keywords:** integrated-optics; wavefront control; infrared; high contrast imaging; high angular resolution; optical fibers; long baseline interferometry; exoplanets; active galactic nuclei; protoplanetary disk; spectroscopy

Paper 22119G received Dec. 6, 2022; revised May 6, 2023; accepted Jun. 6, 2023; published Jun. 27, 2023.

## 1 Introduction

The emphatic triumph of the very large telescope interferometer (VLTI) of the European Southern Observatory (ESO) and its second-generation instruments [namely General Relativity Analysis via Vlt InTerferometrY (GRAVITY)[1] and Multi AperTure mid-Infrared SpectroScopic Experiment][2] in delivering unique science[3–5] has set European astronomy apart. It also motivates the ongoing facility upgrade within the GRAVITY+ framework,[6] promising further groundbreaking scientific discoveries. In parallel, major technology and scientific milestones have been achieved at other interferometric facilities, such as the Center for High Angular Resolution Astronomy array (CHARA) and the Large Binocular Telescope Interferometer (LBTI). New ideas and laboratory demonstrations have also emerged in recent years, opening and enabling the path to novel scientific capabilities for optical interferometry. Leveraging these recent developments, the Asgard instrument suite will extend the scientific capabilities of the VLTI following its priorities for the next decade.[7] This suite is the new visitor instrument of the VLTI, serving as a critical new platform for testing and launching future innovations to deliver benefits to a broad community for years to come. Asgard was submitted for approval to the Science and Technical Committee of ESO during the first semester of 2023 for integration and commissioning from 2024 to mid-2026. The Asgard suite mainly consists of four instruments, which are HEIMDALLR (High-Efficiency Multiaxial Do-it ALL Recombiner), Baldr, BIFROST (Beam-combination Instrument for studying the Formation and fundamental paRameters of Stars and planeTary systems), and NOTT (Nulling Observations of dusT and planeTs). HEIMDALLR and Baldr are mostly dedicated to correcting atmospheric aberrations and atmospheric pistons; BIFROST and NOTT are mostly science-driven. Asgard will operate from Y to L bands (1 to 4 microns). This paper presents the instruments of Asgard, their capabilities, and the key scientific objectives.

## 2 Instrumental Overview

### 2.1 Description of the Modules

Asgard will be located on the Visitor 2 table, formerly the AMBER table (Fig. 1). The conceptual layout of Asgard is given in Fig. 2. In addition to the four instrument modules, Asgard has two common modules. The first one is the Asgard calibration and alignment unit (ACAU), which contains a light source for spectral calibration and a 4-beam coherent light source for internal alignment and cophasing. It operates via pickoffs that are flippable mirrors to select between light from ACAU and the VLTI.

The second common module is the Asgard common optics (ACO), in which the four 18-mm beams from the VLTI (bottom right) are first reflected on the beam compressors (ASG-BC), which reduce the beam size to 12 mm using off-axis parabolas. Four deformable mirrors (ASG-DM) are located in the pupil plane between the two sets of mirrors of the beam compressors. Next, the beams encounter a dichroic (ASG-DIC) that transmits the L band to NOTT and reflects the Y to K bands to the other modules.

Wavelengths from Y to K bands arrive in the HEIMDALLR instrument,[8] a dual-band and multiaxial beam combiner. The beams first go through a dichroic and a periscope (HEI-DIPER). The former separates the Y-J-H bands from the K band. The periscope sends the Y-J-H band to Baldr/BIFROST injection module (BIF-INJ) at the upper level. The K band is transmitted toward the focus and alignment mirrors (HEI-FA) of HEIMDALLR. They are comprised of four pairs of mirrors to align and cophase HEIMDALLR. These optics send the beams to the pupil reconfiguration (HEI-COMB) that encompasses knife-edge mirrors to reconfigure the beams into a

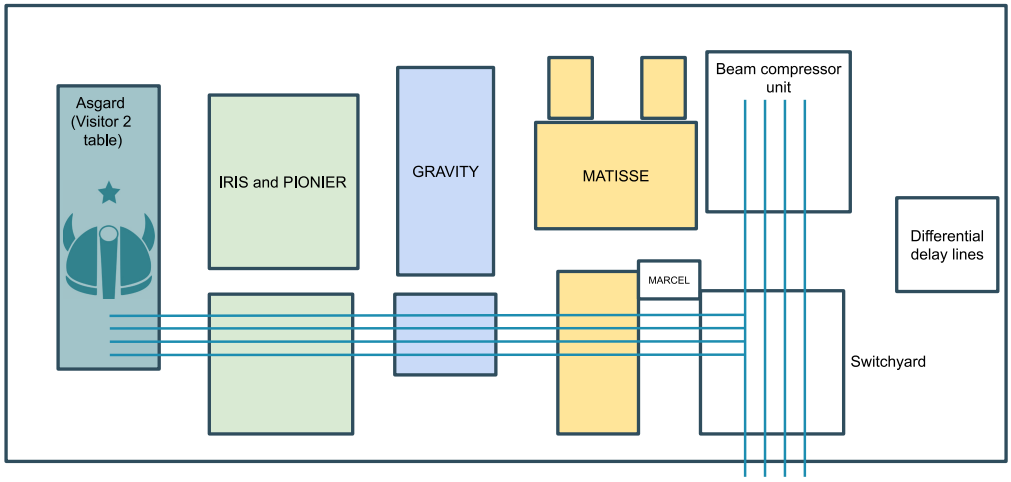


**Fig. 1** Layout of the VLTI lab with the instruments and particularly Asgard at the end of the beam train.

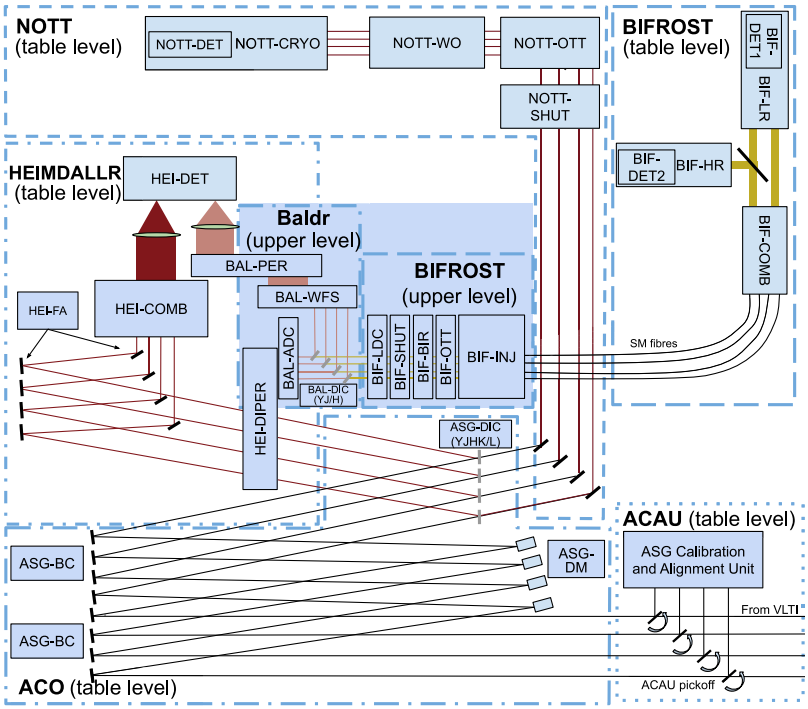


**Fig. 2** Conceptual layout of Asgard. This diagram is not to scale and the positions of the modules are subject to change but the order of the optical components should remain the same.

two-dimensional interferometric pattern analogous to an aperture-masking interferometer. This configuration delivers: the acquisition of astrophysical data, the low order wavefront control by retaining the full two-dimensional information contained in the interferogram, high sensitivity using bulk optics, and closure-phase. The instrument is integrated into a feedback loop with Baldr (see below) and DM to perform fringe tracking (i.e., stabilize the interferometric signal by compensating the differential atmospheric piston)[9] and the correction of higher aberration modes to control the injection into BIFROST and NOTT. However, the stroke of the DM does not allow a correction of the optical path difference (OPD) higher than 10 $\mu$m; hence part of the OPD drift will be offloaded on the VLTI delay lines.

On the upper level, the beams arrive at the Baldr instrument. Baldr provides a Zernike wavefront sensor to augment the capabilities of the new adaptive optics module for interferometry (NAOMI, in the number of modes and speed) or GRAVITY+ adaptive optics (GPAO, in speed

for low-order modes). Its main goal is to maximize the injection of light into the photonic components of BIFROST and NOTT. It can operate in either J or H bands, leaving the rest of Y, J, or H for BIFROST science.

The beams first go through the Atmospheric Dispersion Compensation (BAL-ADC) made of four pairs of prisms. These devices will compensate for the chromatic dispersion effect between the Y and H bands, which degrades the injection efficiency and induces differential phases. Then Baldr's dichroic (BAL-DIC) reflects the H-band to Baldr's wavefront sensors optics (BAL-WFS) and transmits the J-Y band to BIFROST. An alternative beam splitter can also be translated instead to reflect the J band to Baldr and transmit the H band to BIFROST. The BAL-WFS is a Zernike phase sensor that decomposes the wavefront on a Zernike aberration base. Next, a periscope (BAL-PER) sends the signal from the wavefront sensor to the HEIMDALLR's camera.

Meanwhile, the rest of the beams split by the BAL-DIC are sent to BIFROST,[10,11] which is a photonic long-baseline interferometer. In a nutshell, long-baseline interferometry coherently combines the light from two telescopes to provide an image with a higher angular resolution than that provided by a single-dish telescope.[9] BIFROST will offer new and complementary benefits to the second-generation VLTI instruments, namely access to a higher angular resolution (due to shorter wavelengths), a higher continuum flux for blue sources (as we observe closer to the peak wavelength of the photosphere), and a spectral resolution roughly six times greater ($R = 25,000$) than what is currently available at the VLTI. It will also give access to new line tracers, including Pa$\beta$ 1.282 $\mu$m, Pa$\gamma$ 1.094 $\mu$m, the He I 1.083 $\mu$m accretion-tracing line,[12] and forbidden lines [e.g., (Fe II) 1.257 $\mu$m].

The beams within BIFROST first encounter longitudinal dispersion compensators (BIF-LDC) to correct for the atmospheric longitudinal dispersion. Then they go through BIFROST's shutters (BIF-SHUT) that can individually close each beam or all of them to perform the calibration tasks or protect the detectors from bright light while BIFROST is not operating. The shutters are followed by the birefringence correction plates (BIF-BIR), which are made of lithium niobate (LiNbO3). They compensate for the birefringence of the beam trains and the guided optics. The OPD & Tip-Tilt alignment mirrors (BIF-OTT) aim to cophase the input beams between BIFROST and HEIMDALLR and to optimize the light injection into BIFROST injection module (BIF-INJ). This module comprises off-axis paraboloids (OAPs) and fiber tips. The fiber tips receive the light to transport it to the combiner of BIFROST (BIF-COMB) through single-mode fibers. The fiber tips are fixed at the focus of the OAPs. The fibers carry the beams to the BIF-COMB. The combiner is an integrated-optics chip that coherently combines the beams. It also contains a 90/10 beam splitter that can be moved in to record data simultaneously with BIFROST's Low-Resolution arm (BIF-LR) and High-Resolution arm (BIF-HR).[13] The former comprises imaging optics, a prism for low-spectral dispersion at a fixed resolving power ($R = 50$ to 80), and a camera. Also, it contains a Wollaston prism on a translation stage that can be moved in to measure separate polarization states to improve the calibration of the visibility. The low-resolution (LR) arm measures OPD drift, dispersion, and fringe jumps to feed a feedback loop on the longitudinal dispersion compensators (LDC) and the BIFROST differential delay lines. The high-resolution (HR) arm comprises imaging optics, a filter wheel with grisms for high spectral dispersion of the fringe pattern, and a camera. It is used for measuring wavelength-differential quantities and closure phases. Both arms have BIFROST detectors (BIF-DET1 and BIF-DET2) to image their respective fringe patterns.

Meanwhile, the L-band beams split by ASG-DIC are sent to NOTT.[14] NOTT will be the first nulling instrument at the VLTI, the first long-baseline nuller in the Southern hemisphere, and the first operating at the L band, where young giant planets are the most luminous. In a nutshell, nulling interferometry suppresses the on-axis light (e.g., from a star) by coherently combining the light from two apertures to create a destructive interference while transmitting the off-axis light (e.g., from a planet).[15] Leveraging the long baseline of the VLTI and the ongoing GRAVITY+ facility upgrade, it will be able to directly image the snow line where most giant exoplanets are located.[16,17]

The beams first encounter the beam conditioner (NOTT-SHUT) that comprises shutters and diaphragms. It shuts the beams individually for calibration purposes and equalizes the beam intensities to optimize the null depth. Then, the OPD and TT alignment mirrors (NOTT-OTT) cophase the beams between NOTT and HEIMDALLR and optimize the light injection into the photonic chip. After, the beams go through the NOTT warm optics. They comprise LDC,

polarization control optics, the slicer, and the alignment camera. The LDC compensates for the chromatic phase across the L band and the water vapor effects via a feedback loop. The polarization control compensates for polarization effects, which reduce the instrumental null depth. The slicer[18] overlaps the four telescope pupils on the cold stop at the entrance of the NOTT cryostat (NOTT-CRYO). The cryostat contains a window, a cold stop, the photonic chip[19] that combines the beams and creates photometric outputs, a spectrograph[20] and imaging optics, the camera (NOTT-DET), the cryocooler, and the vacuum system. The chip's design is based on the double-Bracewell architecture.[21,22] The spectrograph contains grisms for different spectral resolutions. The camera collects the spectrally-dispersed signal delivered by the photonic chip. In addition, NOTT will be able to compensate for fringe drifts due to water vapor and $CO_2$ dispersion. To do so, it will rely on the simultaneous analyses of its signal with the wavefront analysis of HEIMDALLR and the telemetry of BIFROST.

This structure allows HEIMDALLR and Baldr to always be operated simultaneously with either BIFROST or NOTT. For some common targets of the two scientific instruments, simultaneous observations of the four modules would be possible.

### 2.2 Optomechanical Design

The conceptual layout (Fig. 2) has yielded a preliminary optomechanical design to verify that Asgard can fit on the VLTI optical table (Fig. 3). The beams of the VLTI enter on the left-hand

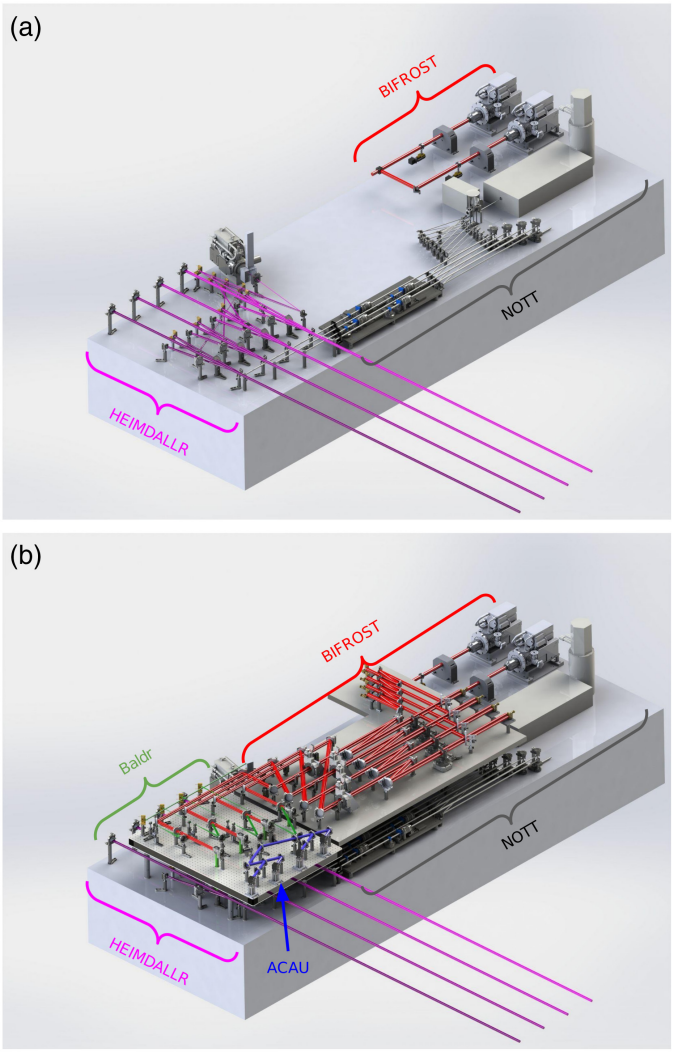


**Fig. 3** Preliminary version of the optomechanical design of Asgard: (a) table level and (b) full design. The optical paths are colored for each module: HEIMDALLR (purple), BIFROST (red), NOTT (gray), Baldr (green), and ACAU (blue).

side of the Visitor 2 table and come across ACO and HEIMDALLR's paths on the lower level and are split between the different instruments as previously described (Sec. 2.1). This preliminary design demonstrates the possibility of fitting four full-scale instruments into a single optical table.

### 2.3 Control Architecture

The overall Asgard control architecture is given in Fig. 4. The hardware architecture is designed so that two terminals can operate all the modules. These terminals can connect to the observing workstation (observing WS) on Asgard through the ESO network. This centralization allows the observer to run all the instruments simultaneously and to communicate with the VLTI systems. Moreover, this structure enables information sharing between the modules. It is particularly critical to optimize the correction brought by the DMs during fringe tracking and to compensate for dispersions effects (longitudinal, atmospheric, water vapor, and $CO_2$).

Asgard's computers hardware and software are non-ESO compliant, hence must be kept separate. However, Asgard modules need to interact with ESO systems, such as the delay lines or IRIS via the reflective memory network (RMN), the variable curvature mirror, the fast steering mirror, and the Multi-beam Alignment, Reference and Calibration Emitter for the Laboratory (MARCEL) for the laboratory via the Interferometric Supervisor Software (ISS). The suggested solution is to create a local network on which the IT components of each module are connected: the Asgard internal network called Yggdrasil. The users run Asgard systems through the observing WS that is accessed either directly (during in-laboratory operations) or via the terminals (during the observations). An ESO-link WS, called Hermod, connected to Yggdrasil, will interact with the ESO network, be directly plugged into the RMN, and transmit data to and from Asgard modules as required. It is also connected to the Asgard archive to store Asgard data acquired over several weeks. In a future extension, the Asgard archive could also serve as the hub for feeding Asgard data into the ESO archive. Hermod will respect ESO's standards for hardware and software. From the ESO network point of view, Asgard is a unique computer represented by Hermod.

Each module has one or two local control units (LCU) or programmable logic controllers (PLC) to drive Asgard's sub-systems and components, including monitor cameras, science detectors, and the piezo-actuators. The LCUs are connected to the Asgard internal network and are driven from the terminals. The PLCs directly control the optomechanical components and are controlled by the terminals similarly to the LCUs. Each module (except ACAU) has its own data storage embedded in its respective LCU.

The LCUs managing the detectors have direct access to the archive to write the frames, and the user can access the storage via the observing WS. The connections between the WS and LCUs are made with ethernet cables and the Transistor-Transistor Logic (TTL) protocol.

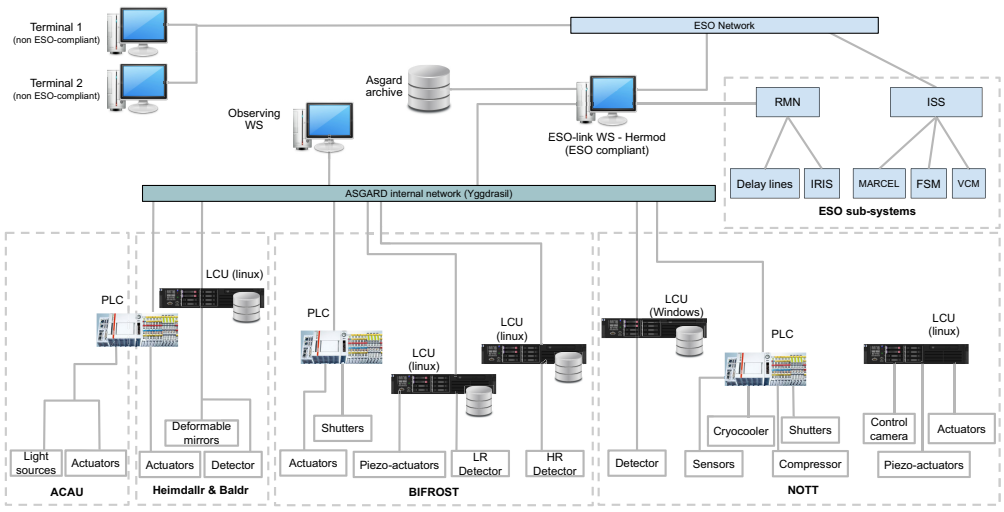


**Fig. 4** Preliminary Control architecture of Asgard.

The instrument software package will be subdivided into the following software modules:

- The instrument control software (ICS): controls all devices connected to the LCU on which it is installed, except the detector. There will be one ICS per module.
- The detector control software (DCS): controls the detector. There will be one DCS per LCU connected to a detector.
- The observing software (OS): coordinates the acquisitions of the instrument, interfaces with the ESO-link WS, with the local storage disk space of the modules, and the Asgard archive.
- The link software: exchanges information and instructions between ESO and Asgard networks.

### 2.4 Data Flow

The data flow is shown in Fig. 5. Asgard will use its own observing blocks, which will be based on ESO's template. After each observing night, the data (in FITS format) and the observing logs are copied to the local Asgard database. The data and the logs are copied to different places depending on the instrument (BIFROST data sent to the University of Exeter, HEIMDALLR/Baldr sent to the Australian National University and NOTT data sent to the Katholieke Universiteit Leuven). The transfer would be done by physically moving the storage drives. The data are reduced, and quality control checked. Reduced data are formatted in OIFITS files to be published and put on the Jeam-Marie Mariotti Center's optical interferometry database, along with their observing logs.

## 3 Instrument Capabilities

The main instrumental features of the VLTI Asgard science modules are given in Table 1, and preliminary performance estimates are presented in Table 2.

## 4 Science Cases for Asgard

Asgard science cases are diverse and mostly revolve around stellar physics, multiple systems, and exoplanetary science.[10,14] Asgard will first focus on well-chosen targets to assess its capabilities; then, it will operate in survey mode and address all the science cases below.

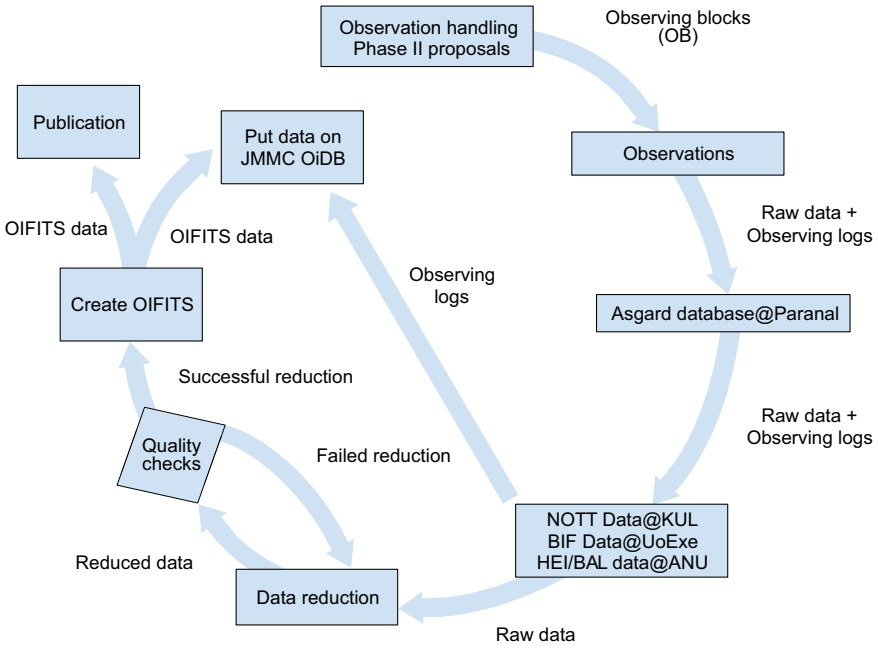


**Fig. 5** Preliminary data flow plan of Asgard.

**Table 1** Main instrumental features of the VLTI Asgard modules.

| Feature | HEIMDALLR | Baldr | BIFROST | NOTT |
|---|---|---|---|---|
| Photometric band | K | H | Y, J, H | L |
| Central wavelength ($\mu$m) | 2.18 | 1.6 | 1.35 | 3.75 |
| Bandwidth ($\mu$m) | 0.45 | 0.3 | 0.6 | 0.5 |
| Spectral resolutions | $R = 5$ (two channels) | None | LR arm: $R = 50, 100, 1500, 5000$ (Y, J, H) | $R = 20$ |
| | | | HR arm (Y, J): $R = 1000$ (1.05 to 1.65 $\mu$m) | $R = 400$ |
| | | | HR: $R = 5000$ (1.05 to 1.65 $\mu$m) | $R = 2000$ |
| | | | VHR: $R = 25{,}000$ (around He I + Pa$\beta$ and Pa$\gamma$) | |
| Polarization split | NO | — | YES (optional) | YES[a] |
| Off-axis mode | — | — | YES[a] | — |
| Inner working angle @3.75 $\mu$m | — | — | — | 2 mas (AT)[b], 3 mas (UT)[c] |
| Diameter of the field of view | 250 mas (AT)[b], 55 mas (UT)[c] | 183 mas (AT)[b], 41 mas (UT)[c] | 155 mas (AT)[b], 34 mas (UT)[c] | 430 mas (AT)[b], 94 mas (UT)[c] |
| Interferometric observable | $V^2$, closure phase | — | $V^2$, closure phase, differential phases | Null depth, differential null depth |
| Magnitude limit | $K = 11.5$ (ATs)[b] or 13.5 (UTs)[c] | $H = 9.6$ (ATs)[b] or 12.9 (UTs)[c] | Limited by Baldr | $L' = 11$ (ATs)[b] or 13 (UTs)[c] |

[a]Contingent on additional funding.
[b]Auxiliary telescope.
[c]Unit telescope.

**Table 2** Preliminary performance of the VLTI Asgard modules.

| Feature | HEIMDALLR | Baldr | BIFROST | NOTT |
|---|---|---|---|---|
| Precision on $V^2$ | 5% | — | 3% (LR arm) | — |
| Precision on closure phase | 1 deg | — | 0.5 deg (LR arm) | — |
| Precision on differential phase | — | — | 0.1 deg(HR arm) | — |
| Residual piston RMS (nm) | <100 (UT)<br><50 (AT) | — | — | — |
| Strehl (in J band) | — | >50% (AT)<br>>40% (UT) | — | — |
| RMS intensity fluctuations (in L band) | — | <2% | — | — |
| Precision on null depth ($L = 4$ and $R = 18$) | — | — | — | $5 \times 10^{-5}$ (UT)<br>$3 \times 10^{-4}$ (AT) |

### 4.1 Formation Process of Binary Systems

The Data Release 3 of the Gaia mission provides roughly 813,000 non-single stars.[23] Gaia's radial velocity spectrometer also provides precision radial velocities. Around 357,000 of these systems are detected through astrometry and as double-lined spectroscopic binary.[23] However, with an angular resolution of 0.1 arcsecond, Gaia is not able to spatially resolve most of these systems. Thus, there is a degeneracy between the flux ratio of the components and their separations. BIFROST and HEIMDALLR will aim to spatially resolve and characterize up to 6000 binaries among these 357,000 systems[10] via the measurements of visibilities, closure phases, and differential phases. They will find the statistics of orbital parameters by solving the degeneracy of the Gaia measurement of the photocenter. Combined with statistics from radial velocity observations and direct imaging, this data will help constrain the formation process of binary systems. These instruments will also allow for the derivation of the dynamical masses of such binary systems. Thus, they will provide inputs for the refinement of evolutionary models that are the cornerstone of modern astrophysics, as these models currently face uncertainties, for instance, the treatment of mass-loss in massive stars.[24,25] The uncertainties are particularly notable in the pre-main-sequence phase, where predicted and measured masses currently differ by $\geq 10\%$.[26] HEIMDALLR and BIFROST will measure the binary flux ratio in the K band and Y/J band, respectively. BIFROST's operating wavelengths are close to the Gaia band (0.4 to 0.9 $\mu$m). This will enable the derivation of dynamical masses with a precision of $\sim 3\%$. The mass constraint will also give access to the ages of the stars, which is important for galactic archaeology studies. Finally, BIFROST will give information about the processes involved in the formation and dynamical evolution of binaries and planetary systems by measuring the spin-orbit alignment of the binaries and planet-host stars. This is achieved through BIFROST's very high-spectral resolution (VHR) mode with $R = 25,000$ ($\Delta v \sim 12$ km/s), which enables the measuring of the stellar spin orientation in moderate/slow rotating stars. The statistics obtained from these observations will enable tests of theories concerning the origin of this obliquity, such as multiple modes of formation, the Kozai-Lidov mechanism or the flyby of neighboring stars.

### 4.2 Mass Accretion and Ejection

BIFROST will also have a particular interest in studying the process of mass accretion and ejection from young stellar objects (YSO) and active galactic nuclei (AGN).[10] It will bring new contributions[10] to previous studies about accretion disks around T Tauri stars,[27] disk winds around Herbie Ae/Be stars,[28] wind-wind collision in luminous-blue variables,[29] relativistic jets in micro-quasars[30] and AGNs.[31] To do so, the instrument will perform differential visibility measurements in the Paschen lines and the He I 1.083 $\mu$m line; these are stronger markers than Br$\gamma$ lines in the K band.[32] Thus, it will gather critical information on accretion disks, wind-wind collisions, disk winds, and relativistic jets from micro-quasars. In addition, by spatially and

spectrally resolving multiple transitions of hydrogen recombination lines, BIFROST can constrain the physical conditions (gas density, temperature, excitation) and the velocity field at different regions in the circumstellar environment. This will enable new approaches for the reconstruction of the three-dimensional velocity field in the inner regions of protoplanetary disks, where accretion occurs, and winds are launched from the star, the disk, or the interaction region between the stellar and disk magnetic fields.

### 4.3 Formation and Evolution of Exoplanetary Systems and Exoplanet Atmospheres

One of the main scientific goals of NOTT is to characterize the chemical composition of known giant exoplanets discovered by radial velocity or expected to be found soon with the new release of the astrometric measurements made with Gaia (~25% of planets more massive than $\sim 0.3 M_{\mathrm{Jup}}$ present in nearby moving groups[33]). These exoplanets are located in uncharted territory, i.e., close to the water ice line, which is inaccessible to current direct-imaging instruments and future extremely large telescopes (ELTs). Although the Gaia mission provides valuable information about the masses of giant gas exoplanets and the ages of the systems, it only brings partial knowledge about the formation and evolution of exoplanetary systems. By measuring the effective temperatures of the exoplanets,[14] NOTT will constrain their planet-formation models[34] better. The NOTT exoplanet target list currently includes nearly 1500 young stars (<250 Myr) within 150 pc. By selecting the best star candidates ($\approx$ 20 stars) thanks to Monte-Carlo simulations and end-to-end simulations,[35–37] NOTT can potentially detect 5 to 10 giant exoplanets, depending on the planet-formations models (core accretion or gravitational instability).

NOTT's spectroscopic capability will enable us to trace the thermal emission from these exoplanets, opacities of absorbers (molecular bands, dust, clouds),[14] and BIFROST will be able to probe the exoplanet atmospheres using its off-axis mode,[10] in particular those of Jupiter-like exoplanets. They will give access to critical information about the non-equilibrium chemistry of their atmosphere, their vertical temperature profiles, atmospheric dynamics, rotation rates, and formation processes. Comparing the chemical composition of these gaseous objects with the composition of their migrated and more distant siblings probed through transit (e.g., with the James Webb Space Telescope) and single-dish direct imaging will help clarify the role played by migration by extreme irradiation on gaseous planets.

### 4.4 Protoplanetary and Circumplanetary Disks

Protoplanetary disks are structured with rings, gaps, spirals, and large cavities that provide clues about the formation process. The observed cavities are often large (>20 AU) and are observed in 10% of the disks,[38] and many of them show asymmetric features, such as spirals or vortices[39] that are linked to the presence of companions carving the cavities in the disk.[40] NOTT observations will provide new inputs for hydrodynamical models to understand planet-disk interaction and constrain planet formation and evolution in the very early stages. The high-contrast nulling mode of NOTT combined with the long VLTI baselines will provide the dynamic range and angular resolution required to observe the cavities of transition disks imaged at shorter wavelengths by current direct imaging instruments such as the Spectro-Polarimetric High-Contrast Exoplanet Research (SPHERE), currently inaccessible to other L-band (single-dish) exoplanet imagers.

BIFROST's high-resolution spectroscopic capability will probe the circumplanetary disks where exoplanets are formed.[10] The instrument will investigate the Pa$\gamma$ and Pa$\beta$ lines for PDS70c-like protoplanets in the circumplanetary disk, thereby revealing the kinematics in the circumplanetary disk and the accretion onto the forming planets. This capability complements GRAVITY's K-band off-axis mode for atmospheric retrieval studies that will face ambiguities otherwise (e.g., see Table 3 of Ref. 41). In addition, the James Webb Space Telescope, the Atacama Large Millimeter/submillimeter Array, and the Mid-infrared ELT Imager and Spectrograph on the ELT will likely discover new PDS70c-like protoplanets around young stars, whose circumplanetary disks can be characterized with BIFROST. NOTT will enable image reconstruction and thus a detailed study of the origin of the dust through its distribution, in addition to the previously mentioned structures showing planet-disk interaction.[14]

### 4.5 Exozodiacal Dust

Exozodiacal dust is warm and hot dust located in the inner regions of main-sequence planetary systems, near the habitable zone (HZ) and closer in.[42] It presents both a scientific interest and an obstacle for a future imaging survey for exo-Earths and the spectroscopic search for biosignatures in their atmospheres. Scientifically, the dust can act as a tracer for the architecture, dynamics, and evolution of its host planetary and planetesimal system.[43–46] For exo-Earth imaging, the light from HZ dust adds photon noise to the observations and causes confusion from potential disk structures.[47] Exozodiacal dust has so far only been observed in thermal emission due to the lower dust-to-star contrast compared to scattered light. However, the dust's excess emission is still too faint to detect photometrically. Thus, it needs to be spatially resolved from the star, and the small angular scales and high contrasts involved (1 AU at 10 parsecs corresponds to 0.1") require precision interferometry.[48] Particularly, nulling interferometry on the VLTI with NOTT will provide tenfold better sensitivity to extended circumstellar emission than stellar interferometers like the Precision Integrated-Optics Near-infrared Imaging ExpeRiment (PIONIER)[49,50] and the Fiber Linked Unit for Optical Recombination (FLUOR).[51,52] In addition, the dust-to-star contrast is by a factor of ∼5 more favorable in the L band than in H band.[53] To do so, NOTT will rely on high contrast circumstellar emission detection, similar to what has been done with VLTI/PIONIER.[50] This will be done on the ATs using the polarization corrector of NOTT.

## 5 Conclusion

Asgard is a new instrument suite accepted by ESO (P110, March 2022) as a visitor instrument to open new unique scientific capabilities at the VLTI (YJH high-spectral resolution and L-band high-contrast nulling interferometry at milli-arcsecond angular separation). It consists of 4 different modules: BIFROST (YJH high-spectral resolution, $R = 50$, 1000, 5000, 25,000), Baldr (Zernike Wavefront Sensor, H band), HEIMDALLR (high-sensitivity fringe tracker, dual K band), and NOTT (L band, 3.5 to 4 microns, nulling interferometer). The suite is currently in the design and preparation phases. The design aims to make the instruments interoperable and their data integrated into the existing data flow of ESO in the long term.

### Acknowledgments

M.-A.M. has received funding from the European Union's Horizon 2020 research and innovation program (Grant No. 101004719). S.K. and S.C. acknowledge support from an ERC Consolidator Grant ("GAIA-BIFROST," Grant No. 101003096). S.K. and D.J.M. acknowledge support from STFC (Grant No. ST/V000721/1). SCIFY (A.B., C.D., D.D., G.G., and R.L.) has received funding from the European Research Council (ERC) under the European Union's Horizon 2020 research and innovation program (Grant No. CoG - 866070). We are grateful for the kind support and constructive interactions with colleagues at ESO, in particular Frédéric Gonte, Xavier Haubois, Antoine Mérand, Nicolas Schuhler, and Julien Woillez. This research was partially funded by the Australian Government through the Australian Research Council (Grant No. LE220100126).

### References

1. F. Eisenhauer et al., "GRAVITY: observing the universe in motion," *Messenger* **143**, 16–24 (2011).
2. B. Lopez et al., "MATISSE, the VLTI mid-infrared imaging spectro-interferometer," *A&A* **659**, A192 (2022).
3. R. Abuter et al., "Detection of the Schwarzschild precession in the orbit of the star S2 near the Galactic centre massive black hole," *A&A* **636**, L5 (2020).
4. GRAVITY Collaboration, S. Lacour et al., "First direct detection of an exoplanet by optical interferometry. Astrometry and K-band spectroscopy of HR 8799 e," *A&A* **623**, L11 (2019).
5. V. Gámez Rosas et al., "Thermal imaging of dust hiding the black hole in NGC 1068," *Nature* **602**, 403–407 (2022).
6. GRAVITY Collaboration, R. Abuter et al., "The GRAVITY+ Project: towards all-sky, faint-science, high-contrast near-infrared interferometry at the VLTI," *Messenger* **189**, 17–22 (2022).
7. A. Mérand, "The VLTI roadmap," *Messenger* **171**, 14–19 (2018).
8. M. J. Ireland et al., "Image-plane fringe tracker for adaptive-optics assisted long baseline interferometry," *Proc. SPIE* **10701**, 1070111 (2018).

9. P. Lawson, *Principles of Long Baseline Stellar Interferometry*, National Aeronautics and Space Administration, Jet Propulsion Laboratory, California Institute of Technology (2000).
10. S. Kraus et al., "High spectral-resolution interferometry down to one micron with Asgard/BIFROST at VLTI: science drivers and project overview," *Proc. SPIE* **12183**, 121831S (2022).
11. D. J. Mortimer et al., "Beam combiner for the Asgard/BIFROST instrument," *Proc. SPIE* **12183**, 121831U (2022).
12. W. Fischer et al., "Redshifted absorption at He I λ 10830 as a probe of the accretion geometry of T Tauri stars," *ApJ* **687**, 1117–1144 (2008).
13. S. Chhabra et al., "Spectrograph design for the Asgard/BIFROST spectro-interferometric instrument for the VLTI," *Proc. SPIE* **12183**, 121830M (2022).
14. D. Defrère et al., "L-band nulling interferometry at the VLTI with Asgard/Hi-5: status and plans," *Proc. SPIE* **12183**, 121830H (2022).
15. R. N. Bracewell, "Detecting nonsolar planets by spinning infrared interferometer," *Nature* **274**, 780–781 (1978).
16. R. B. Fernandes et al., "Hints for a turnover at the snow line in the giant planet occurrence rate," *ApJ* **874**, 81 (2019).
17. B. J. Fulton et al., "California legacy survey. II. Occurrence of giant planets beyond the ice line," *ApJS* **255**, 14 (2021).
18. G. Garreau et al., "Design of the VLTI/Hi-5 light injection system," *Proc. SPIE* **12183**, 1218320 (2022).
19. A. Sanny et al., "Development of the four-telescope photonic nuller of Hi-5 for the characterization of exoplanets in the mid-IR," *Proc. SPIE* **12183**, 1218316 (2022).
20. C. Dandumont et al., "Technical requirements and optical design of the Hi-5 spectrometer," *Proc. SPIE* **12183**, 121831Y (2022).
21. J. R. P. Angel and N. J. Woolf, "An imaging nulling interferometer to study extrasolar planets," *ApJ* **475**, 373–379 (1997).
22. R. Errmann et al., "Interferometric nulling of four channels with integrated optics," *Appl. Opt.* **54**, 7449 (2015).
23. Gaia Collaboration, A. Vallenari et al., "GAIA data release 3: summary of the content and survey properties," arXiv:2208.00211 (2022).
24. G.A. Feiden and B. Chaboyer, "Reevaluating the mass-radius relation for low-mass, main-sequence stars," *ApJ* **757**, 42 (2012).
25. A. W. Mann et al., "How to constrain your M Dwarf: measuring effective temperature, bolometric luminosity, mass, and radius," *ApJ* **804**, 64 (2015).
26. K. G. Stassun, G. A. Feiden, and G. Torres, "Empirical tests of pre-main-sequence stellar evolution models with eclipsing binaries," *New A Rev.* **60**, 1–28 (2014).
27. GRAVITY Collaboration, R. Garcia Lopez et al., "A measure of the size of the magnetospheric accretion region in TW Hydrae," *Nature* **584**, 547–550 (2020).
28. E. Hone et al., "Gas dynamics in the inner few AU around the Herbig B[e] star MWC297. Indications of a disk wind from kinematic modeling and velocity-resolved interferometric imaging," *A&A* **607**, A17 (2017).
29. G. Weigelt et al., "VLTI-AMBER velocity-resolved aperture-synthesis imaging of η Carinae with a spectral resolution of 12 000. Studies of the primary star wind and innermost wind-wind collision zone," *A&A* **594**, A106 (2016).
30. GRAVITY Collaboration, R. Abuter et al., "First light for GRAVITY: phase referencing optical interferometry for the very large telescope interferometer," *A&A* **602**, A94 (2017).
31. GRAVITY Collaboration, E. Sturm et al., "Spatially resolved rotation of the broad-line region of a quasar at sub-parsec scale," *Nature* **563**, 657–660 (2018).
32. C. P. Nicholls et al., "CRIRES-POP: a library of high resolution spectra in the near-infrared. II. Data reduction and the spectrum of the K giant 10 Leonis," *A&A* **598**, A79 (2017).
33. A. L. Wallace, M. J. Ireland, and C. Federrath, "Constraints on planets in nearby young moving groups detectable by high-contrast imaging and GAIA astrometry," *MNRAS* **508**, 2515–2523 (2021).
34. A. L. Wallace and M. J. Ireland, "The likelihood of detecting young giant planets with high-contrast imaging and interferometry," *MNRAS* **490**, 502–512 (2019).
35. C. Dandumont et al., "VLTI/Hi-5: detection yield predictions for young giant exoplanets," *Proc. SPIE* **12183**, 1218327 (2022).
36. R. Laugier et al., "Asgard/nott: L-band nulling interferometry at the vlti - i. simulating the expected high-contrast performance," *A&A* **671**, A110 (2023).
37. R. Laugier et al., "The expected performance of nulling at the VLTI down to five mas," *Proc. SPIE* **12183**, 1218321 (2022).
38. N. van der Marel et al., "New insights into the nature of transition disks from a complete disk survey of the lupus star-forming region," *ApJ* **854**, 177 (2018).

39. N. van der Marel et al., "On the diversity of asymmetries in gapped protoplanetary disks," *ApJ* **161**, 33 (2021).
40. B. J. Norfolk et al., "Dust traps and the formation of cavities in transition discs: a millimetre to sub-millimetre comparison survey," *MNRAS* **502**, 5779–5796 (2021).
41. GRAVITY Collaboration, M. Nowak et al., "Peering into the formation history of β Pictoris b with VLTI/GRAVITY long-baseline interferometry," *A&A* **633**, A110 (2020).
42. Q. Kral et al., "Exozodiacal clouds: hot and warm dust around main sequence stars," *Astron. Rev.* **13**, 69–111 (2017).
43. V. Faramaz et al., "Inner mean-motion resonances with eccentric planets: a possible origin for exozodiacal dust clouds," *MNRAS* **465**, 2352–2365 (2017).
44. A. Bonsor et al., "Using warm dust to constrain unseen planets," *MNRAS* **480**, 5560–5579 (2018).
45. J. K. Rigley and M. C. Wyatt, "Dust size and spatial distributions in debris discs: predictions for exozodiacal dust dragged in from an exo-Kuiper belt," *MNRAS* **497**, 1143–1165 (2020).
46. D. Defrère et al., "The HOSTS survey: evidence for an extended dust disk and constraints on the presence of giant planets in the habitable zone of $\beta$ Leo," *ApJ* **161**, 186 (2021).
47. D. Defrère et al., "Direct imaging of exoEarths embedded in clumpy debris disks," *Proc. SPIE* **8442**, 84420M (2012).
48. S. Ertel et al., "The HOSTS survey for exozodiacal dust: observational results from the complete survey," *ApJ* **159**, 177 (2020).
49. J. B. Le Bouquin et al., "PIONIER: a 4-telescope visitor instrument at VLTI," *A&A* **535**, A67 (2011).
50. S. Ertel et al., "A near-infrared interferometric survey of debris-disk stars. IV. An unbiased sample of 92 southern stars observed in H band with VLTI/PIONIER," *A&A* **570**, A128 (2014).
51. V. Coudé du Foresto et al., "FLUOR fibered beam combiner at the CHARA array," *Proc. SPIE* **4838**, 280–285 (2003).
52. N. J. Scott et al., "Jouvence of FLUOR: upgrades of a fiber beam combiner at the CHARA array," *J. Astron. Instrum.* **2**, 1340005 (2013).
53. F. Kirchschlager et al., "First L band detection of hot exozodiacal dust with VLTI/MATISSE," *MNRAS* **499**, L47–L52 (2020).


Biographies of the authors are not available.